

Radiation-induced magnetoresistance oscillations in two-dimensional electron systems under bichromatic irradiation

X. L. Lei

Department of Physics, Shanghai Jiaotong University, 1954 Huashan Road, Shanghai 200030, China

We analyze the magnetoresistance R_{xx} oscillations in high-mobility two-dimensional electron systems induced by the combined driving of two radiation fields of frequency ω_1 and ω_2 , based on the balance-equation approach to magnetotransport for high-carrier-density systems in Faraday geometry. It is shown that under bichromatic irradiation of $\omega_2 \sim 1.5\omega_1$, most of the characteristic peak-valley pairs in the curve of R_{xx} versus magnetic field in the case of monochromatic irradiation of either ω_1 or ω_2 disappear, except the one around $\omega_1/\omega_c \sim 2$ or $\omega_2/\omega_c \sim 3$. R_{xx} oscillations show up mainly as new peak-valley structures around other positions related to multiple photon processes of mixing frequencies $\omega_1 + \omega_2$, $\omega_2 - \omega_1$, etc. Many minima of these resistance peak-valley pairs can descend down to negative with enhancing radiation strength, indicating the possible bichromatic zero-resistance states.

PACS numbers: 73.50.Jt, 73.40.-c, 78.67.-n, 78.20.Ls

I. INTRODUCTION

Since the discovery of radiation induced magnetoresistance oscillations (RIMOs) and zero-resistance states (ZRS) in ultra-high mobility two-dimensional (2D) electron systems,^{1,2,3,4} tremendous experimental^{5,6,7,8,9,10,11,12,13,14} and theoretical^{15,16,17,18,19,20,21,22,23,24,25,26,27,28,29,30,31,32,33,34} efforts have been devoted to study this exciting phenomenon and a general understanding of it has been reached. Under the influence of a microwave radiation of frequency $f = \omega/2\pi$, the low-temperature magnetoresistance R_{xx} of a 2D electron gas (EG), exhibits periodic oscillation as a function of the inverse magnetic field. The RIMOs feature the periodical appearance of peak-valley pairs around $\omega/\omega_c = 1, 2, 3, 4, \dots$, i.e. a maximum at $\omega/\omega_c = j - \delta_j^-$ and a minimum at $\omega/\omega_c = j + \delta_j^+$, with $j = 1, 2, 3, 4, \dots$ and $0 < \delta_j^\pm \leq 1/4$. Here ω_c is the cyclotron frequency and $\omega/\omega_c = j$ are the node points of the oscillation. With increasing the radiation intensity the amplitudes of the peak-valley oscillations increase and the resistance R_{xx} around the minima of a few lowest- j pairs can drop down towards negative direction but will stop when a vanishing resistance is reached, i.e. ZRS.

In addition to these basic features, secondary peak-valley pair structures were also observed experimentally^{3,4,6,7,8,11,13} and predicted theoretically^{23,31} around $\omega/\omega_c = 1/2, 3/2$ and $2/3$. They were referred to the effect of two- and three-photon processes and their minima were shown also to be able to develop into negative value when increasing the radiation further.²³ Recent measurement at 27 GHz with intensified microwave intensity,¹⁴ confirmed these multiphoton-related peak-valley pairs and the ZRSs developed from their minima. A careful theoretical analysis with enhanced radiation convincingly reproduced these structures and predicted more peak-valley pairs related to multiphoton processes.³⁵

Despite intensive experimental and theoretical studies have been done in the case of monochromatic irradiation, further investigations beyond this configuration are highly desirable for a deeper understanding of this fascinating phenomenon. An easy way is to study the response of the 2D system to a bichromatic radiation, which apparently can not be reduced simply to the superposition of the system response to each monochromatic radiation. Thus the presence of a second radiation of different frequency could provide additional insight into the problem of microwave-driven 2D electron system.

Theoretically, effect of a bichromatic irradiation on transport of a 2D electron gas was investigated within a model of a clean classical gas, in which Kohn's theorem is violated entirely due to nonparabolicity without invoking Landau quantization.³⁶ Some features that are specific to the bichromatic case, such as new domain of magnetic field within which the diagonal conductivity is negative, were revealed.

Experimentally, Zudov *et al.*¹⁴ recently measured the magnetoresistance of a high-mobility 2D electron system under the combined driving of two radiation fields of frequency ω_1 and ω_2 , and disclosed features of RIMOs which are quite different from those under monochromatic radiation of frequency ω_1 or ω_2 . They detected a new resistance minimum under bichromatic microwave radiation, which seems to originate from a frequency mixing process, possibly a precursor of bichromatic ZRS.

In this paper we report our studies on microwave photoresistance response of high-mobility two-dimensional electron systems under bichromatic irradiation, based on the balance-equation approach to magnetotransport for high-carrier-density systems, extended to the case of simultaneous driving of two radiation fields of different frequencies. The balance-equation approach, though semiclassical in nature, has been shown to capture the essence of this radiation-induced nonlinear magnetotransport quantitatively.^{23,31} Under bichromatic irradiation of $\omega_2 \sim 1.5\omega_1$, we find that most of the characteristic peak-valley pairs in the curve of R_{xx} versus magnetic

field in the case of monochromatic irradiation of either ω_1 or ω_2 disappear, except the one around $\omega_1/\omega_c \sim 2$ or $\omega_2/\omega_c \sim 3$. R_{xx} oscillations show up mainly as new peak-valley structures around other positions related to multiple photon processes of mixing frequencies $\omega_1 + \omega_2$, $\omega_2 - \omega_1$, etc.

II. BALANCE EQUATIONS UNDER BICHROMATIC RADIATION

The derivation of balance equations under bichromatic radiation follows that of monochromatic radiation.³¹ The nature of the balance-equation approach and its applicability to radiation-driven magnetotransport in high-mobility 2D electron systems of high carrier density, was examined closely in Ref. 31. We refer the readers to it for detail.

In the case of bichromatic radiation we consider that a dc or slowly time-varying electric field \mathbf{E}_0 and two high frequency (HF) fields

$$\mathbf{E}_1(t) \equiv \mathbf{E}_{1s} \sin(\omega_1 t) + \mathbf{E}_{1c} \cos(\omega_1 t) \quad (1)$$

and

$$\mathbf{E}_2(t) \equiv \mathbf{E}_{2s} \sin(\omega_2 t) + \mathbf{E}_{2c} \cos(\omega_2 t) \quad (2)$$

are applied simultaneously in a quasi-2D system consisting of N_e interacting electrons in a unit area of the x - y plane, together with a magnetic field $\mathbf{B} = (0, 0, B)$ along the z direction. The frequencies ω_1 and ω_2 are high enough and their difference is large enough that ω_1 and ω_2 , as well as $|n_1\omega_1 - n_2\omega_2|$ (for arbitrary integers n_1 and n_2), are all much larger than $1/\tau_0$, where τ_0 stands for the scale of the time variation of slowly varying field \mathbf{E}_0 , or the time scale within which one carries out the transport measurement, whichever the shorter. The approach is based on the separation of the center-of-mass motion from the relative electron motion of the electrons and describes the transport state of a high-carrier-density many-electron system under radiation fields in terms of a rapidly time-varying electron drift velocity oscillating at both base radiation frequencies, $\mathbf{v}(t) = \mathbf{v}_1(t) + \mathbf{v}_2(t)$, with

$$\mathbf{v}_1(t) = \mathbf{v}_{1c} \cos(\omega_1 t) + \mathbf{v}_{1s} \sin(\omega_1 t), \quad (3)$$

$$\mathbf{v}_2(t) = \mathbf{v}_{2c} \cos(\omega_2 t) + \mathbf{v}_{2s} \sin(\omega_2 t), \quad (4)$$

together with another part \mathbf{v}_0 for the slowly varying electron drift motion, as well as an electron temperature T_e characterizing the electron heating.^{37,38} In the case of ultra-clean electron gas at low temperatures, the slowly time-varying quantities \mathbf{v}_0 and T_e satisfy the following force- and energy-balance equations:^{23,31}

$$m \frac{d\mathbf{v}_0}{dt} = e\mathbf{E}_0 + e(\mathbf{v}_0 \times \mathbf{B}) + \frac{\mathbf{F}_0}{N_e}, \quad (5)$$

$$N_e \mathbf{E}_0 \cdot \mathbf{v}_0 + S_p - W = 0, \quad (6)$$

with \mathbf{v}_{1c} and \mathbf{v}_{1s} determined by

$$-m\omega_1 \mathbf{v}_{1c} = e\mathbf{E}_{1s} + e(\mathbf{v}_{1s} \times \mathbf{B}), \quad (7)$$

$$m\omega_1 \mathbf{v}_{1s} = e\mathbf{E}_{1c} + e(\mathbf{v}_{1c} \times \mathbf{B}); \quad (8)$$

and \mathbf{v}_{2c} and \mathbf{v}_{2s} determined by

$$-m\omega_2 \mathbf{v}_{2c} = e\mathbf{E}_{2s} + e(\mathbf{v}_{2s} \times \mathbf{B}), \quad (9)$$

$$m\omega_2 \mathbf{v}_{2s} = e\mathbf{E}_{2c} + e(\mathbf{v}_{2c} \times \mathbf{B}). \quad (10)$$

Here e and m are the electron charge and effective mass,

$$\mathbf{F}_0 = \sum_{\mathbf{q}_{\parallel}} |U(\mathbf{q}_{\parallel})|^2 \sum_{n_1, n_2 = -\infty}^{\infty} J_{n_1}^2(\xi_1) J_{n_2}^2(\xi_2) \times \mathbf{q}_{\parallel} \Pi_2(\mathbf{q}_{\parallel}, \omega_0 - n_1\omega_1 - n_2\omega_2) \quad (11)$$

is the damping force of the moving center-of-mass,

$$S_p = \sum_{\mathbf{q}_{\parallel}} |U(\mathbf{q}_{\parallel})|^2 \sum_{n_1, n_2 = -\infty}^{\infty} J_{n_1}^2(\xi_1) J_{n_2}^2(\xi_2) \times (n_1\omega_1 + n_2\omega_2) \Pi_2(\mathbf{q}_{\parallel}, \omega_0 - n_1\omega_1 - n_2\omega_2) \quad (12)$$

is the averaged rate of the electron energy absorption from the HF fields, and

$$W = \sum_{\mathbf{q}} |M(\mathbf{q})|^2 \sum_{n_1, n_2 = -\infty}^{\infty} J_{n_1}^2(\xi_1) J_{n_2}^2(\xi_2) \times \Omega_{\mathbf{q}} \Lambda_2(\mathbf{q}, \omega_0 + \Omega_{\mathbf{q}} - n_1\omega_1 - n_2\omega_2) \quad (13)$$

is the average rate of the electron energy dissipation to the lattice. In the above equations, $J_{n_1}(\xi_1)$ and $J_{n_2}(\xi_2)$ are Bessel functions of order n_1 and n_2 , $\xi_1 \equiv \sqrt{(\mathbf{q}_{\parallel} \cdot \mathbf{v}_{1c})^2 + (\mathbf{q}_{\parallel} \cdot \mathbf{v}_{1s})^2}/\omega_1$, $\xi_2 \equiv \sqrt{(\mathbf{q}_{\parallel} \cdot \mathbf{v}_{2c})^2 + (\mathbf{q}_{\parallel} \cdot \mathbf{v}_{2s})^2}/\omega_2$, and $\omega_0 \equiv \mathbf{q}_{\parallel} \cdot \mathbf{v}_0$. Here $q_{\parallel} \equiv (q_x, q_y)$ stands for the in-plane wavevector, $U(\mathbf{q}_{\parallel})$ is the effective impurity scattering potential, and $\Pi_2(\mathbf{q}_{\parallel}, \Omega)$ is the imaginary part of the electron density correlation function of the quasi-2D system in the magnetic field. In Eq. (13), \mathbf{q} represents the 3D wavevector $(\mathbf{q}_{\parallel}, q_z)$ plus the branch index λ , and the summation is for all possible 3D phonon modes of frequency $\Omega_{\mathbf{q}}$ having electron-phonon scattering matrix element $M(\mathbf{q})$. $\Lambda_2(\mathbf{q}, \Omega) = 2\Pi_2(\mathbf{q}_{\parallel}, \Omega)[n(\Omega_{\mathbf{q}}/T) - n(\Omega/T_e)]$ (with $n(x) \equiv 1/(e^x - 1)$) is the imaginary part of the electron-phonon correlation function. The $\Pi_2(\mathbf{q}_{\parallel}, \Omega)$ function of a 2D system in a magnetic field can be expressed in the Landau representation:³⁹

$$\Pi_2(\mathbf{q}_{\parallel}, \Omega) = \frac{1}{2\pi l_B^2} \sum_{n, n'} C_{n, n'} (l_B^2 q_{\parallel}^2 / 2) \Pi_2(n, n', \Omega), \quad (14)$$

$$\Pi_2(n, n', \Omega) = -\frac{2}{\pi} \int d\varepsilon [f(\varepsilon) - f(\varepsilon + \Omega)] \times \text{Im}G_n(\varepsilon + \Omega) \text{Im}G_{n'}(\varepsilon), \quad (15)$$

where $C_{n,n+l}(Y) \equiv n![(n+l)!]^{-1}Y^l e^{-Y}[L_n^l(Y)]^2$ with $L_n^l(Y)$ the associate Laguerre polynomial, $l_B \equiv \sqrt{1/|eB|}$ is the magnetic length, $f(\varepsilon) = \{\exp[(\varepsilon - \mu)/T_e] + 1\}^{-1}$ is the Fermi distribution function at electron temperature T_e . The density of states of the n -th Landau level is modeled with a Gaussian form:⁴⁰

$$\text{Im}G_n(\varepsilon) = -(\sqrt{2\pi}/\Gamma) \exp[-2(\varepsilon - \varepsilon_n)^2/\Gamma^2], \quad (16)$$

having a half-width

$$\Gamma = \left(\frac{8e\omega_c\alpha}{\pi m\mu_0} \right)^{1/2} \quad (17)$$

around the level center $\varepsilon_n = n\omega_c$. Here $\omega_c = eB/m$ is the cyclotron frequency, μ_0 is the linear mobility at lattice temperature T in the absence of the magnetic field, and α is a semi-empirical parameter to take account of the difference of the transport scattering time τ_m determining the mobility μ_0 , from the single particle lifetime τ_s related to Landau level broadening.

For time-independent \mathbf{v}_0 , we immediately deduce the transverse and longitudinal dc resistivities from Eq. (5):

$$R_{xy} = B/N_e e, \quad (18)$$

$$R_{xx} = -\mathbf{F}_0 \cdot \mathbf{v}_0 / (N_e^2 e^2 v_0^2). \quad (19)$$

The (linear) magnetoresistivity is its $\mathbf{v}_0 \rightarrow 0$ limit:

$$R_{xx} = -\frac{1}{N_e^2 e^2} \sum_{\mathbf{q}_{\parallel}} q_{\parallel}^2 |U(\mathbf{q}_{\parallel})|^2 \times \sum_{n_1, n_2 = -\infty}^{\infty} J_{n_1}^2(\xi_1) J_{n_2}^2(\xi_2) \left. \frac{\partial \Pi_2}{\partial \Omega} \right|_{\Omega = n_1 \omega_1 + n_2 \omega_2}. \quad (20)$$

We assume that the 2DEG is contained in a thin sample suspended in vacuum at plane $z = 0$. When both electromagnetic waves illuminate upon the plane perpendicularly with the incident electric fields $\mathbf{E}_{i1}(t) = \mathbf{E}_{i1s} \sin(\omega_1 t) + \mathbf{E}_{i1c} \cos(\omega_1 t)$ and $\mathbf{E}_{i2}(t) = \mathbf{E}_{i2s} \sin(\omega_2 t) + \mathbf{E}_{i2c} \cos(\omega_2 t)$, the HF electric fields in the 2DEG, determined by the electrodynamic equations, are

$$\mathbf{E}_1(t) = \frac{N_e e \mathbf{v}_1(t)}{2\epsilon_0 c} + \mathbf{E}_{i1}(t), \quad (21)$$

$$\mathbf{E}_2(t) = \frac{N_e e \mathbf{v}_2(t)}{2\epsilon_0 c} + \mathbf{E}_{i2}(t). \quad (22)$$

Using this $\mathbf{E}_1(t)$ in Eqs. (7) and (8), and $\mathbf{E}_2(t)$ in Eqs. (9) and (10), the oscillating velocity \mathbf{v}_{1c} and \mathbf{v}_{1s} (and thus the argument ξ_1) are explicitly expressed in terms of incident field \mathbf{E}_{i1s} and \mathbf{E}_{i1c} , and the oscillating velocity \mathbf{v}_{2c} and \mathbf{v}_{2s} (and thus the argument ξ_2) are explicitly expressed in terms of incident field \mathbf{E}_{i2s} and \mathbf{E}_{i2c} . Therefore, in the case of weak measuring current limit ($v_0 \rightarrow 0$) we need only to solve the energy balance equation $S_p - W = 0$ to obtain the electron temperature T_e

under given incident radiation fields, before directly calculating the linear magnetoresistivity from Eq. (20).

Within certain field range, the magnetoresistivity R_{xx} given by Eq. (19) can be negative at small v_0 , but will change towards the positive direction with increasing v_0 and passes through zero at a finite v_0 ,²³ implying that the time-independent small-current solution is unstable and a spatially nonuniform¹⁹ or a time-dependent solution³⁴ may develop, which exhibits measured zero resistance. Therefore we identify the region where a negative dissipative magnetoresistance develops as that of the ZRS.

The summations over n_1 and n_2 in Eqs. (11), (12) and (13) include all possible electron transition processes assisted by real and virtual photons of frequency ω_1 and ω_2 . The $n_1 > 0$ terms represent all possible electron transitions with simultaneous absorption of n_1 photons of frequency ω_1 , while $n_1 < 0$ terms represent all possible electron transitions with simultaneous emission of $|n_1|$ photons of frequency ω_1 . We call these electron transitions the $|n_1|$ ω_1 -photon assisted processes. The same for $|n_2|$ ω_2 -photon assisted processes. The $n_1 = 0$ terms represent electron transitions assisted by virtual ω_1 -photons (all possible emission and absorption of same number of ω_1 -photons), and $n_2 = 0$ terms represent electron transitions assisted by virtual ω_2 -photons.

III. NUMERICAL RESULTS

As indicated by experiments,⁴¹ in ultra-clean GaAs-based 2D samples having mobility of order of $10^3 \text{ m}^2/\text{Vs}$, the remote donor scattering is responsible for merely $\sim 10\%$ or less of the total momentum scattering rate. The dominant contribution to the momentum scattering comes from short-range scatterers such as residual impurities or defects in the background. Therefore, as in Ref. 31, we assume that the dominant elastic scatterings contributing to the resistance and energy absorption are due to short-range impurities randomly distributed throughout the GaAs region in the numerical calculations. The impurity densities are determined by the requirement that electron total linear mobility at zero magnetic field equals the giving value at lattice temperature T . Since RIMO measurements are at low temperatures, the direct phonon contributions to S_p and \mathbf{F}_0 (R_{xx}) can be neglected. Nevertheless, to calculate the electron energy dissipation to the lattice, W , we take account of scatterings from bulk longitudinal acoustic (LA) and transverse acoustic (TA) phonons (via the deformation potential and piezoelectric couplings), as well as from longitudinal optical (LO) phonons (via the Fröhlich coupling) in the GaAs-based system. The relevant material and coupling parameters are taken typical values of GaAs:⁴² electron effective mass $m = 0.068 m_e$ (m_e is the free electron mass), transverse sound speed $v_{st} = 2.48 \times 10^3 \text{ m/s}$, longitudinal sound speed $v_{sl} = 5.29 \times 10^3 \text{ m/s}$, acoustic deformation potential $\Xi = 8.5 \text{ eV}$, piezoelectric constant $e_{14} = 1.41 \times 10^9 \text{ V/m}$, dielectric constant

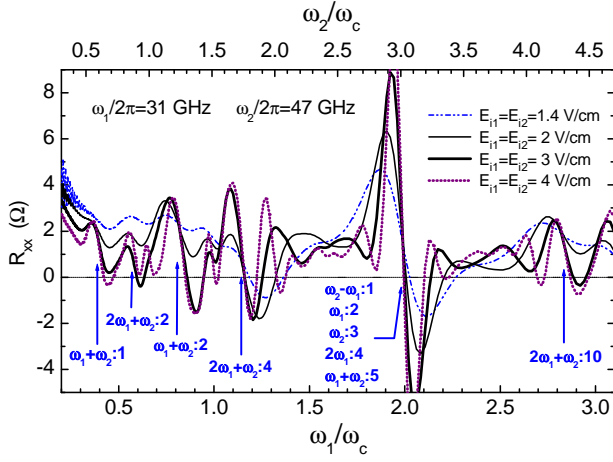


FIG. 1: (Color online) The magnetoresistivity R_{xx} versus the inverse magnetic field $1/B$ for a GaAs-based 2DEG with $N_e = 3.0 \times 10^{15} \text{ m}^{-2}$, $\mu_0 = 2000 \text{ m}^2/\text{Vs}$ and $\alpha = 5$, irradiated simultaneously by two microwaves with frequencies $\omega_1/2\pi = 31 \text{ GHz}$ and $\omega_2/2\pi = 47 \text{ GHz}$ having four sets of incident amplitudes $E_{i1} = E_{i2} = 1.4, 2, 3,$ and 4 V/cm at lattice temperature $T = 1 \text{ K}$. $\omega_c = eB/m$ is the cyclotron frequency at the magnetic field B .

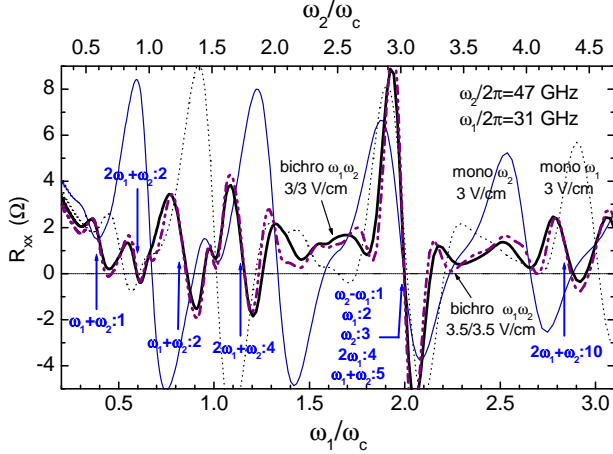


FIG. 2: (Color online) The magnetoresistivity R_{xx} versus the inverse magnetic field $1/B$ for the same system as described in Fig. 1. The thin curves are under monochromatic irradiation either of frequency $\omega_1/2\pi = 31 \text{ GHz}$ and incident amplitude $E_i = 3 \text{ V/cm}$ (dot curve), or of frequency $\omega_1/2\pi = 47 \text{ GHz}$ and incident amplitude $E_i = 3 \text{ V/cm}$ (solid curve). The thick curves are under bichromatic irradiation of frequencies $\omega_1/2\pi = 31 \text{ GHz}$ and $\omega_2/2\pi = 47 \text{ GHz}$ having incident amplitudes $E_{i1} = E_{i2} = 3 \text{ V/cm}$ (solid curve) or 3.5 V/cm (dash-dot curve). The lattice temperature is $T = 1 \text{ K}$.

$\kappa = 12.9$, material mass density $d = 5.31 \text{ g/cm}^3$.

The numerical calculations are performed for x -direction (parallel to \mathbf{E}_0) linearly polarized incident microwave fields $[\mathbf{E}_{i1s} = (E_{i1}, 0), \mathbf{E}_{i1c} = 0$ and $\mathbf{E}_{i2s} = (E_{i2}, 0), \mathbf{E}_{i2c} = 0]$.

Figure 1 shows the calculated magnetoresistivity R_{xx} versus the inverse magnetic field for a GaAs-based 2D

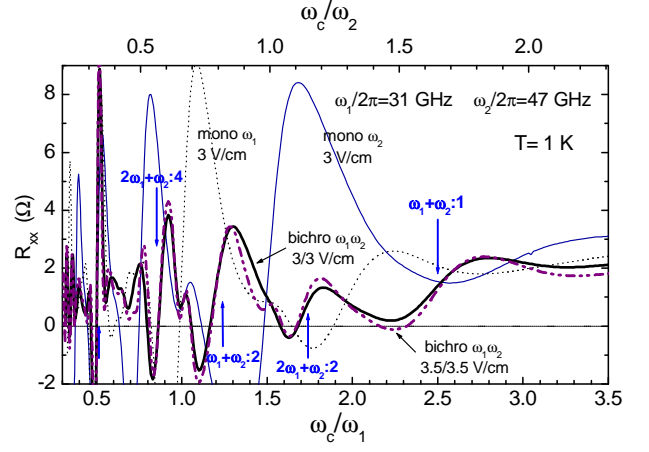


FIG. 3: (Color online) The same as Fig. 2, but magnetoresistivity R_{xx} is shown as a function of the magnetic field B .

system having electron density $N_e = 3.0 \times 10^{15} \text{ m}^{-2}$, linear mobility $\mu_0 = 2000 \text{ m}^2/\text{Vs}$ and broadening parameter $\alpha = 5$, simultaneously irradiated by two microwaves of frequencies $\omega_1/2\pi = 31 \text{ GHz}$ and $\omega_2/2\pi = 47 \text{ GHz}$ with four sets of incident amplitudes $E_{i1} = E_{i2} = 1.4, 2, 3,$ and 4 V/cm at lattice temperature $T = 1 \text{ K}$. We see that the bichromatic photoresponse of R_{xx} is unlike that of monochromatic irradiation. Most of the characterizing peak-valley pairs in the curve of R_{xx} versus magnetic field subjected to monochromatic irradiation of either ω_1 or ω_2 disappear. The only exception is the peak-valley pair around $\omega_1/\omega_c \sim 2$ or $\omega_2/\omega_c \sim 3$, which, on the contrary, is somewhat enhanced in bichromatic irradiation. New peak-valley pairs appear. Their amplitudes generally increase with increasing the incident field strengths as indicated in the figure. Most of these pairs exhibit essentially fixed node positions while growing amplitudes and their minima can drop down into negative.

As in the case of monochromatic illumination, the appearance of magnetoresistance oscillation in the bichromatic irradiation comes from real photon-assisted electron transitions between different Landau levels as indicated in the summation of the electron density-correlation function in Eq. (14). Apparently, all multiple photon processes related to ω_1 monochromatic radiation and ω_2 monochromatic radiation are included. In addition, there are multiple photon processes related to mixing ω_1 and ω_2 radiation.

With three positive integers n_1, n_2 and l to characterize a multiple photon assisted electron transition, we use the symbol $n_1\omega_1 + n_2\omega_2 : l$ to denote a process during which an electron jumps across l Landau level spacings with simultaneous absorption of n_1 photons of frequency ω_1 and n_2 photons of frequency ω_2 , or simultaneous emission of n_1 photons of frequency ω_1 and n_2 photons of frequency ω_2 ; and use the symbol $n_1\omega_1 - n_2\omega_2 : l$ to denote a process during which an electron jumps across l Landau level spacings with simultaneous absorption of n_1 photons of frequency ω_1 and emission of n_2 photons of

frequency ω_2 , or simultaneous emission of n_1 photons of frequency ω_1 and absorption of n_2 photons of frequency ω_2 (thus the symbol $n_2\omega_2 - n_1\omega_1 : l$ has the same meaning as $n_1\omega_1 - n_2\omega_2 : l$). The symbol $n_1\omega_1 : l$ indicates a process during which an electron jumps across l Landau level spacings with the assistance of n_1 real (emission or absorption) ω_1 -photons and virtual ω_2 -photons. So does the symbol $n_2\omega_2 : l$. We find that the processes represented by $n_1\omega_1 + n_2\omega_2 : l$ contribute, in the R_{xx} -versus- ω_c/ω curve, a structure consisting of a minimum and a maximum on both sides of $\omega_c/\omega_1 = n_1(1 + n_2\omega_2/n_1\omega_1)/l$ or $\omega_c/\omega_2 = n_2(1 + n_1\omega_1/n_2\omega_2)/l$. And those by $n_1\omega_1 - n_2\omega_2 : l$ (assume $n_1\omega_1 > n_2\omega_2$) contribute a minimum-maximum pair around $\omega_c/\omega_1 = n_1(1 - n_2\omega_2/n_1\omega_1)/l$ or $\omega_c/\omega_2 = n_2(n_1\omega_1/n_2\omega_2 - 1)/l$.

From the structure of R_{xx} curves with increasing radiation strength in Fig.1 we can clearly identify several peak-valley pairs characteristic of the bichromatic irradiation. The strongest peak-valley pair is around $\omega_1/\omega_c \sim 2$ or $\omega_2/\omega_c \sim 3$, which can be referred to the joint contribution from single and multiple photon processes with mono- ω_1 , mono- ω_2 and mixing ω_1 and ω_2 , such as $\omega_2 - \omega_1 : 1$, $\omega_1 : 2$, $\omega_2 : 3$, $2\omega_1 : 4$, $\omega_1 + \omega_2 : 5$, \dots . The other peak-valley pairs which are clearly identified include that around $\omega_1/\omega_c \sim 0.4$ referred to $\omega_1 + \omega_2 : 1$, \dots ; that around $\omega_1/\omega_c \sim 0.57$ referred to $2\omega_1 + \omega_2 : 2$, \dots ; that around $\omega_1/\omega_c \sim 0.8$ referred to $\omega_1 + \omega_2 : 2$, \dots ; that around $\omega_1/\omega_c \sim 1.14$ referred to $2\omega_1 + \omega_2 : 4$, \dots ; that around $\omega_1/\omega_c \sim 2.84$ referred to $2\omega_1 + \omega_2 : 10$, \dots . They are indicated in the figure. The minima of all these peak-valley pairs can drop down to negative when increasing the strengths of the radiation field, indicating the possible locations of the bichromatic ZRSs.

To compare the photoresponse under bichromatic radiation with those under monochromatic radiation we plot in Fig.2 the magnetoresistivity R_{xx} versus the inverse magnetic field for the above system under simultaneous irradiation of two microwaves having frequencies $\omega_1/2\pi = 31$ GHz and $\omega_2/2\pi = 47$ GHz with incident amplitudes $E_{i1} = E_{i2} = 3$ and 3.5 V/cm, together with those subjected to single microwave radiation of frequency $\omega_1/2\pi = 31$ GHz with incident amplitude $E_i = 3$ V/cm, or of frequency $\omega_1/2\pi = 31$ GHz with incident amplitude $E_i = 3$ V/cm.

This figure is redrawn in Fig.3 showing R_{xx} as a function of the magnetic field to give a clearer view in the higher magnetic field side. It indicates a possible bichromatic ZRS around $\omega_c/\omega_1 \sim 2.2$ or $\omega_c/\omega_2 \sim 1.5$ arising from R_{xx} dropping to negative at the minimum of the valley-peak pair around $\omega_c/\omega_1 \sim 2.5$ associated with the mixing biphoton process $\omega_1 + \omega_2 : 1$. This result is in agreement with the recent experimental observation on the possible precursor of bichromatic ZRS.¹⁴

Note added: After the acceptance of this paper by Phys. Rev. B, we read a further report of the bichromatic microwave photoresistance measurement.⁴³ The experimental peak/valley positions exhibit a good agreement with the present theoretical results in a wide magnetic field range. Our predicted peaks around $\omega_c/\omega_1 = 0.77, 0.52, 0.37$, and valley at $\omega_c/\omega_1 = 0.33$ (Fig.3), quite accurately ($m = 0.068 m_e$) reproduce the observed peaks around $B \approx 570, 380, 275$ G and the valley around $B \approx 250$ G.

This work was supported by Projects of the National Science Foundation of China and the Shanghai Municipal Commission of Science and Technology.

-
- ¹ M. A. Zudov, R. R. Du, J. A. Simmons, and J. R. Reno, Phys. Rev. B **64**, 201311(R) (2001).
² P. D. Ye, L. W. Engel, D. C. Tsui, J. A. Simmons, J. R. Wendt, G. A. Vawter, and J. L. Reno, Appl. Phys. Lett. **79**, 2193 (2001).
³ R. G. Mani, J. H. Smet, K. von Klitzing, V. Narayana-murti, W. B. Johnson, and V. Umansky, Nature **420**, 646 (2002).
⁴ M. A. Zudov, R. R. Du, L. N. Pfeiffer, and K. W. West, Phys. Rev. Lett. **90**, 046807 (2003).
⁵ C. L. Yang, M. A. Zudov, T. A. Knuutila, R. R. Du, L. N. Pfeiffer, and K. W. West, Phys. Rev. Lett. **91**, 096803 (2003).
⁶ S. I. Dorozhkin, JETP Lett. **77**, 577 (2003).
⁷ R. G. Mani, J. H. Smet, K. von Klitzing, V. Narayana-murti, W. B. Johnson, and V. Umansky, Phys. Rev. Lett. **92**, 146801 (2004).
⁸ R. L. Willett, L. N. Pfeiffer, and K. W. West, Phys. Rev. Lett. **93**, 026804 (2004).
⁹ A. E. Kovalev, S. A. Zvyagin, C. R. Bowers, J. L. Reno, and J. A. Simmons, Solid State Commun. **130**, 379 (2004).
¹⁰ R. G. Mani, Physica E **25**, 189 (2004); Appl. Phys. Lett. **85**, 4962 (2004).
¹¹ M. A. Zudov, Phys. Rev. B **69**, 041304(R) (2004).
¹² S. A. Studenikin, M. Potenski, A. Sachrajda, M. Hilke, L. N. Pfeiffer, and K. W. West, IEEE Tran. on Nanotech. **4**, 124 (2005).
¹³ S. I. Dorozhkin, J. H. Smet, V. Umansky, K. von Klitzing, Phys. Rev. B **71**, 201306(R) (2005).
¹⁴ M. A. Zudov, R. R. Du, L.N. Pfeiffer, and K. W. West, Phys. Rev. B **73**, 041303(R) (2006).
¹⁵ V. I. Ryzhii, Sov. Phys. Solid State **11**, 2087 (1970).
¹⁶ V. I. Ryzhii, R. A. Suris, and B.S. Shchamkhalova, Sov. Phys.-Semicond. **20**, 1299 (1986).
¹⁷ P. W. Anderson and W. F. Brinkman, cond-mat/0302129.
¹⁸ A. A. Koulakov and M. E. Raikh, Phys. Rev. B **68**, 115324 (2003).
¹⁹ A. V. Andreev, I. L. Aleiner, and A. J. Millis, Phys. Rev. Lett. **91**, 056803 (2003).
²⁰ A. C. Durst, S. Sachdev, N. Read, and S. M. Girvin, Phys. Rev. Lett. **91**, 086803 (2003).
²¹ J. Shi and X. C. Xie, Phys. Rev. Lett. **91**, 086801 (2003).
²² I. A. Dmitriev, A. D. Mirlin, and D. G. Polyakov, Phys. Rev. Lett. **91**, 226802 (2003).
²³ X. L. Lei and S. Y. Liu, Phys. Rev. Lett. **91**, 226805 (2003); X. L. Lei, J. Phys.: Condens. Matter **16**, 4045 (2004).

- ²⁴ V. Ryzhii and R. Suris, *J. Phys.: Condens. Matter* **15**, 6855 (2003).
- ²⁵ M. G. Vavilov and I. L. Aleiner, *Phys. Rev. B* **69**, 035303 (2004).
- ²⁶ S. A. Mikhailov, *Phys. Rev. B* **70**, 165311 (2004).
- ²⁷ J. Dietel, L. I. Glazman, F. W. J. Hekking, F. von Oppen, *Phys. Rev. B* **71**, 045329 (2005).
- ²⁸ M. Torres and A. Kunold, *Phys. Rev. B* **71**, 115313 (2005).
- ²⁹ I. A. Dmitriev, M. G. Vavilov, I. L. Aleiner, A. D. Mirlin, and D. G. Polyakov, *Phys. Rev. B* **71**, 115316 (2005).
- ³⁰ J. Iñarrea and G. Platero, *Phys. Rev. Lett.* **94**, 016806 (2005); *Phys. Rev. B* **72**, 193414 (2005).
- ³¹ X. L. Lei and S. Y. Liu, *Phys. Rev. B* **72**, 075345 (2005); *Appl. Phys. Lett.* **86**, 262101 (2005).
- ³² V. Ryzhii, *Jpn. J. Appl. Phys.* **44**, 6600 (2005).
- ³³ C. Joas, J. Dietel, and F. von Oppen, *Phys. Rev. B* **72**, 165323 (2005).
- ³⁴ T. K. Ng and Lixin Dai, *Phys. Rev. B* **72**, 235333 (2005).
- ³⁵ X. L. Lei and S. Y. Liu, *Appl. Phys. Lett.* (at press).
- ³⁶ C. Joas, M. E. Raikh, and F. von Oppen, *Phys. Rev. B* **70**, 235302 (2004).
- ³⁷ X. L. Lei and C. S. Ting, *Phys. Rev. B* **32**, 1112 (1985); X. L. Lei, *J. Appl. Phys.* **84**, 1396 (1998).
- ³⁸ S. Y. Liu and X. L. Lei, *J. Phys.: Condens. Matter* **15**, 4411 (2003).
- ³⁹ C. S. Ting, S. C. Ying, and J. J. Quinn, *Phys. Rev. B* **14**, 5394 (1977).
- ⁴⁰ T. Ando, A. B. Fowler, and F. Stern, *Rev. Mod. Phys.* **54**, 437 (1982).
- ⁴¹ V. Umansky, R. de Picciotto, and Heiblum, *Appl. Phys. Lett.* **71**, 683 (1997).
- ⁴² X. L. Lei, J. L. Birman, and C. S. Ting, *J. Appl. Phys.* **58**, 2270 (1985).
- ⁴³ M. A. Zudov, R. R. Du, L.N. Pfeiffer, and K. W. West, *cond-mat/0605488*.